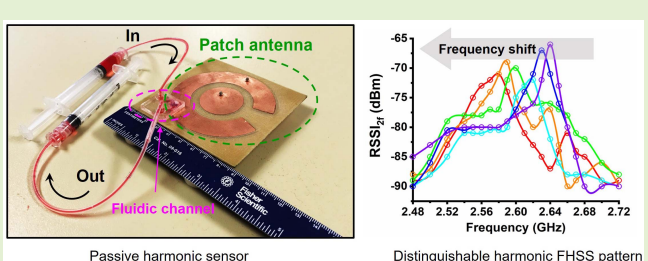


A Compact, Passive Frequency-Hopping Harmonic Sensor Based on a Microfluidic Reconfigurable Dual-Band Antenna

Liang Zhu[®], Graduate Student Member, IEEE, Mohamed Farhat, Yi-Chao Chen[®], Member, IEEE, Khaled N. Salama, Senior Member, IEEE, and Pai-Yen Chen[®], Senior Member, IEEE

Abstract—We propose here a fully-passive wireless liquid sensor using a harmonic transponder, which comprises a dual-band microstrip antenna reconfigured by different types of liquids injected in a fluidic cavity. Different from traditional radio-frequency (RF) backscatter sensors, the proposed harmonic-transponder sensor (or harmonic sensor) receives frequency-hopped RF monotones and backscatters their second harmonics, with the peak frequency shifted by dielectric properties of liquid mixtures. This microstrip antenna has a hybrid-feed structure, of which an outer splitring patch exhibits a narrow-band TM₃₁₀ mode at the fundamental frequency (f_0) and an inner elliptical patch displays a wideband resonance centered at the second-harmonic fre-



quency (2 f_0), achieved with hybridization of TM_{e110} and TM_{o110} modes. In particular, the outer split-ring patch is loaded with a fluidic channel system to tune the resonance frequency of the TM₃₁₀ mode (f_0). We demonstrate that the type of liquid mixture filling in the fluidic cavity can be clearly perceived by reading the peak received signal strength indicator (RSSI) in the spectrum of second harmonics. Our results show the potential for deploying this passive wireless sensor in noisy environments that include clutters, multiple reflections, jamming, and crosstalks.

Index Terms—Antenna sensors, harmonic-transponder sensors, passive wireless sensors, microstrip antennas, clutters, cross talks, electromagnetic interferences.

I. INTRODUCTION

TIRELESS sensing and tracking are core technologies that enable many applications in the scope of internet-of-things (IoT), industrial 4.0, wireless healthcare, and smart city, to name a few [1]-[4]. In most wireless sensing systems, a reader or interrogator transmits a continuous wave (CW) radio-frequency (RF) signal to power a tag and receives backscattered signals that are modulated by a sensor or actuator on the tag [5]–[7]. Along with development

Manuscript received May 7, 2020; revised May 30, 2020; accepted May 31, 2020. Date of publication June 8, 2020; date of current version October 2, 2020. This work is based upon work supported by the National Science Foundation under Grant No. 1914420. The associate editor coordinating the review of this article and approving it for publication was Prof. Sang-Seok Lee. (Corresponding author: Pai-Yen Chen.)

Liang Zhu and Pai-Yen Chen are with the Department of Electrical and Computer Engineering, University of Illinois, Chicago, IL 60607 USA (e-mail: pychen@uic.edu).

Mohamed Farhat and Khaled N. Salama are with the Division of Computer, Electrical, and Mathematical Science and Engineering, King Abdullah University of Science and Technology (KAUST), Thuwal 23955-6900. Saudi Arabia.

Yi-Chao Chen is with the Department of Computer Science and Engineering, Shanghai Jiao Tong University, Shanghai 200240, China. Digital Object Identifier 10.1109/JSEN.2020.3000778

of ubiquitous massive sensors, the ever-increasing wireless nodes and the combination of heterogeneous networks have already generated a time-varying and rich-scattering complex environment filled with echoes, clutters, crosstalks and other electromagnetic interference sources. Very recently, the concept of harmonic sensor was inspired by the concept of harmonic radar, and has gained considerable attention because it provides a longer detection range and an enhanced signalto-noise ratio (SNR) for electrically-small passive wireless sensors [8]-[12]. These harmonic sensors can be classified as nonlinear antenna sensors, whose resonant frequency can be sensitively reconfigured by the dielectric characteristics of the sample under test (SUT) [13]-[16]. Unlike traditional radio-frequency identification (RFID)-based passive sensors, a compact harmonic sensor receives a monotone signal at the fundamental frequency (f_0) and retransmits the modulated high/sub-harmonic signal (nf_0) to monostatic or bistatic readers. By transmitting and detecting RF signals at orthogonal frequencies, this harmonic-based wireless sensing system has the capability to greatly suppress clutters, echo noises, and crosstalks, even though the nonlinear sensor has a small footprint and radar cross-section (RCS). Generally speaking,

1558-1748 © 2020 IEEE. Personal use is permitted, but republication/redistribution requires IEEE permission. See https://www.ieee.org/publications/rights/index.html for more information.

harmonic sensors have been demonstrated to be effective in several applications, such as tracking small-RCS insects or frogs [17]-[21], RECCO avalanche victim searching system [22], and continuous monitoring of biological parameter, humidity, and temperature monitoring [23]-[27]. Despite these widespread applications, until now, harmonic sensors still suffer from several pitfalls. For example, they generally requires dual antennas, i.e., a R_x antenna to receive the fundamental tone (f_0) and a T_x antenna to retransmit the harmonic signal (e.g., second harmonic or $2f_0$) [28], [29], which inevitably increases the overall sensor/tag size and cost. Besides, wireless readout that relies merely on detecting the amplitude of backscattered second harmonic could still struggle with errors and data misinterpretation due to path loss and reflections of second harmonic. Although the widespectrum absolute resonance sensing could address this issue, microstrip antennas used in traditional RFID tags are usually narrowband [28], [29], and, therefore, not suitable for widespectrum applications.

In this paper, we propose a compact, reconfigurable dualband microstrip antenna that can be used for making a lowprofile passive harmonic sensor to monitor liquid density in real time. Specifically, this harmonic sensor adopts the robust wide-spectrum absolute resonance sensing [Fig. 1] that has not yet been explored in existing RFID sensor systems. This antenna excites a narrowband resonant mode at f_0 and a broadband resonance at $2f_0$, which is necessary for the frequency-hopping harmonics-based sensing. In addition, as understood from the eigenmodal analysis, the microstrip antenna is properly loaded with a fluidic cavity such that perturbations caused by the liquid's dielectric properties can shift the resonance frequency f_0 , while not affecting the broadband resonance around $2f_0$. Consequently, a nonlinear, widespectrum absolute resonance sensing scheme can be achieved by analyzing the frequency hopping spread spectrum (FHSS) of the reader, as illustrated in Fig. 1.

In the proposed wireless sensing system, the reader's transceiver (T_x) transmits a constant-strength frequency-hopping sequence with 20 channels $[f_1, f_2,..., f_{20}]$ to the harmonic sensor equipped with the proposed dual-band antenna. These hopping signals are received in sequence by the harmonic sensor, undergoing the frequency doubling process $[f_1, f_2,..., f_{20}] \rightarrow [2f_1, 2f_2,..., 2f_{20}],$ and being retransmitted to the portable sniffer (e.g. smart phone with 5G and LTE antenna covering the frequency band of interest). The dielectric property of the SUT can effectively modulate the antenna's resonance frequency f_0 , which will be extracted by post-processing the high-dimensional FHSS pattern $[2f_1,$ $2f_2 \dots 2f_{20}$], as sketched in Fig. 1. The FHSS pattern analysis can provide robust and accurate absolute resonance sensing, which is not possible with one-dimensional data obtained from traditional non-hopping harmonic RFID sensors.

II. THEORETICAL MODELING OF DUAL-BAND PATCH ANTENNA

We have studied a compact, dual-resonance microstrip antenna composed of a concentric outer split-ring patch and an inner circular patch, which respectively resonate at f_0 (TM₃₁₀

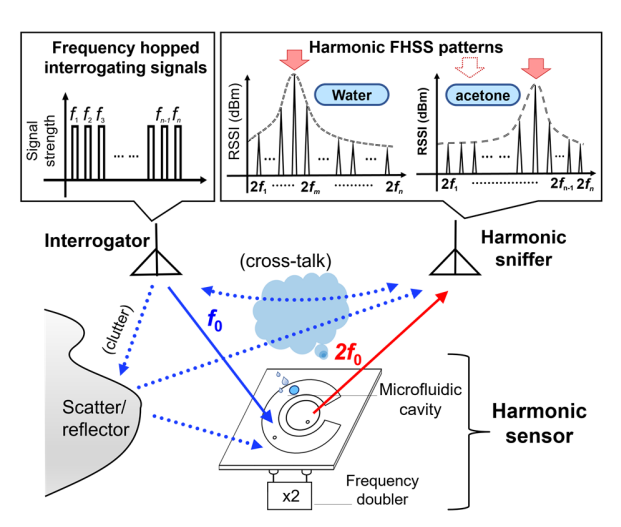


Fig. 1. Schematics and sensing mechanism of a frequency-hopping harmonic sensor based on the proposed dual-band microstrip antenna. The antenna displays a liquid-reconfigured narrow resonance at the fundamental frequency f_0 and an insensitive wideband resonance centering in the second-harmonic band $2f_0$. The full-passive harmonic sensor receives and backscatters RF signals at orthogonal frequencies to avoid clutters and crosstalks. The types of liquids inside the microfluidic cavity can be known by analyzing the frequency hopping spread spectrum (FHSS) pattern.

mode of the split-ring patch antenna) and $2f_0$ (TM₁₁₀ mode of the circular patch antenna), provided that feed points are suitably located [30]. However, both resonant modes have a narrow bandwidth. In order to perform the FHSS analysis, the inner circular patch must be replaced by the geometry that gives a wideband resonance. An elliptical patch with tailorable even and odd resonant modes could be the simplest possible design for effectively increasing the bandwidth around $2 f_0$. Additionally, unlike our previous work utilizing a rectangular patch with a microcavity to perturbate its TM_{010} mode [31], we further integrate the dual-resonance microstrip antenna with a practical fluidic channel loaded with different sampleunder-tests (SUTs). Fig. 2 shows the geometry of the proposed dual-band microstrip antenna consisting of an elliptical patch, a concentric split-ring patch, and a fluidic channel integrated on top. The proposed patch layer is separated from the ground plane by the FR4 substrate with relative permittivity $\varepsilon_r = 4.2$, thickness h = 1.6 mm, and loss tangent $\delta = 0.015$. Given the fact that the antenna has a negligible thickness compared to operating wavelengths, resonance frequencies can be predicted by the cavity model [32]-[34]. In our case, two open cavities with concentric split-ring and elliptical shapes are considered, respectively. The perfect electric conductor (PEC) boundary conditions are applied to top and bottom layers of these two cavities, and the perfect magnetic conductor (PMC) is assumed for their sidewalls. The transcendental equation for the split-ring resonant cavity can be derived as [30]:

$$J'_n(kR_2)Y'_n(kR_3) - J'_n(kR_3)Y'_n(kR_2) = 0,$$

$$n = \frac{m\pi}{2\pi - \theta_0} \text{ for } m = 1, 2, 3 \dots, \quad (1)$$

where $J_n(\cdot)$ and $Y_n(\cdot)$ are the Bessel functions of the first and the second kinds, $k = \omega \sqrt{\varepsilon_r \varepsilon_0 \mu_0}$, ε_0 and μ_0 are the free-space permittivity and permeability. Based on Eq. (1),

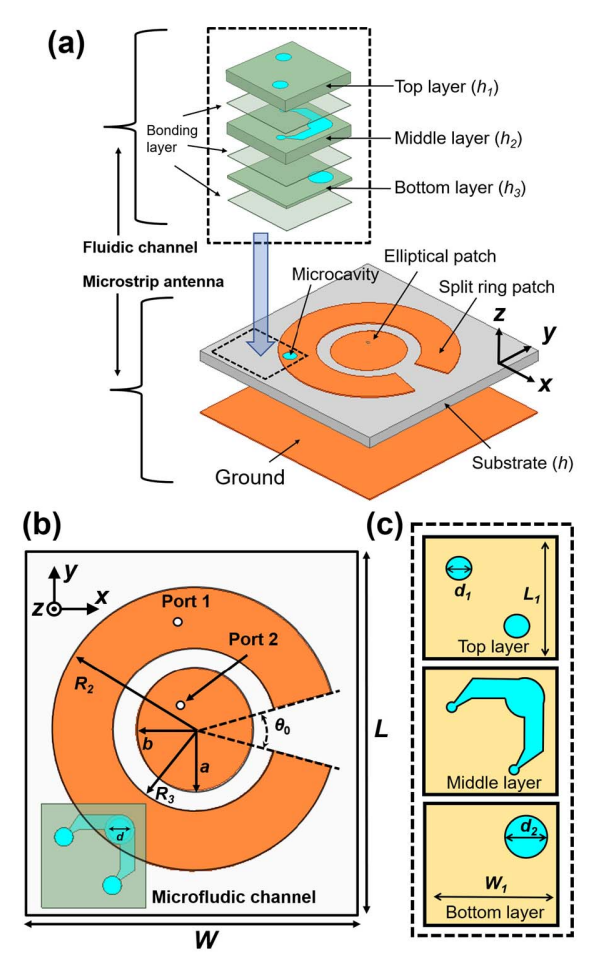


Fig. 2. Geometry and dimensions of the proposed dual band microstrip antenna with fluidic channel: (a) 3-D view. (b) Top view of the microstrip antenna. (c) Top view of the three-layers fluidic channel.

we have designed the split-ring patch antenna with m=3 (TM₃₁₀ mode), $R_2=38.2$ mm, $R_3=22$ mm, and $\theta_0=30^\circ$, which provides a narrow-band resonance at the fundamental frequency (1.31 GHz here).

For the elliptical cavity with the reference elliptical coordinate (ξ, η) , where $\xi \in [0, \infty]$ and $\eta \in [0, 2\pi]$, the transcendental equations can be reduced to the following set, with PMC boundary conditions assumed at the sidewall $\xi = \xi_0[35]$, [36]:

$$M_{e,n}^{\prime(1)}(\xi_0, q) = 0$$
 for *n*-th even mode $M_{e,n}^{\prime(1)}(\xi_0, q) = 0$ for *n*-th odd mode (2)

where $q=c^2k^2/4$, the semi-focal length $c=\sqrt{a^2-b^2}$, $M_{e,n}^{(1)}(\xi,q)$ and $M_{o,n}^{(1)}(\xi,q)$ are respectively the even and odd radial Mathieu function of the first kind, n is the order of the angular Mathieu functions $C_{e,n}(\eta,q)$ and $S_{e,n}(\eta,q)$, which determine the azimuthal variation along η [37], [38]. By solving the above transcendental equation with $\xi_0=1.83$ (a=16.5 mm, and b=15.675 mm), the first even-order mode (TM_{e110} at 2.55 GHz) and the first odd-order mode (TM_{e110} at 2.64 GHz) can be excited in the second-harmonic band for achieving a wideband resonance. We have conducted full-wave numerical simulations [39] to validate the analytical results. Figs. 3(a)-(c) present snapshots of electric field distributions

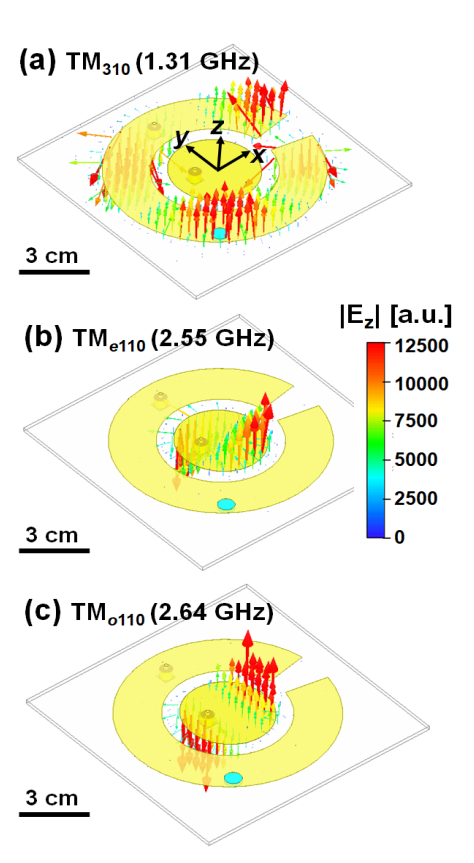


Fig. 3. Simulation results for snapshots of electric field E_z : (a) TM₃₁₀ mode at 1.31 GHz, (b) TM_{e110} mode at 2.55 GHz, and (c) TM_{o110} mode at 2.64 GHz.

for the TM_{310} , TM_{e110} and TM_{o110} modes, respectively. The simulated field distributions are in good agreement with results obtained from the cavity model, showing that the TM_{e110} and TM_{o110} modes exhibit orthogonal modal patterns.

III. EXPERIMENTAL RESULTS

According to the theoretical analysis, we have fabricated the dual-band microstrip antenna based on the FR4 substrate and copper (Cu) microstrips, as shown in Fig. 4. The important design parameters are listed in Table I. In particular, it should be noted that a 50 ohms coaxial cable feed is positioned at x = -5 mm, y = 4.5 mm to simultaneously excite the TM_{e110} (2.55 GHz) and TM_{o110} (2.64 GHz) modes of the elliptical patch. A fluidic cavity with radius r = 2 mm is drilled at position x = -27 mm and y = -20 mm, where the TM₃₁₀ resonant mode exhibits the maximum electric field strength [see Fig. 3(a)]. To accurately control the volume in the microcavity, a fluidic channel consisting of three acrylic layers with thickness h_1 , h_2 and h_3 was fabricated [see Table I]. Each layer was etched into the specific shape [Fig. 2] by using Epilog Mini 24 laser cutter, and all layers were tied together using the double-sided adhesive tape. Subsequently, the assembled fluidic channel was mounted onto the patch antenna and connected with two plastic tubes (i.e., inlet and outlet) [Fig. 4]. Fig. 5 reports the simulated (solid lines) and measured (dashed lines) reflection coefficients versus frequency for this dual-band microstrip antenna. The resonance frequencies calculated using Eqs. (1) and (2) are also highlighted (red stars) here, which agree well with the full-wave

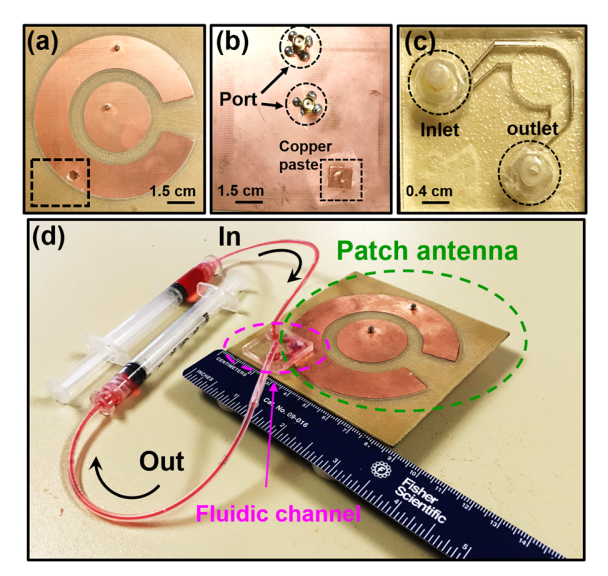


Fig. 4. Photograph of the proposed antenna: (a) Top view of the proposed dual-band patch antenna. The dashed line outlines the area of fluidic channel. (b) Bottom view of the proposed dual-band patch antenna. (c) Top view of the fluidic channel. (d) Integrated passive harmonic sensor with fluidic channel.

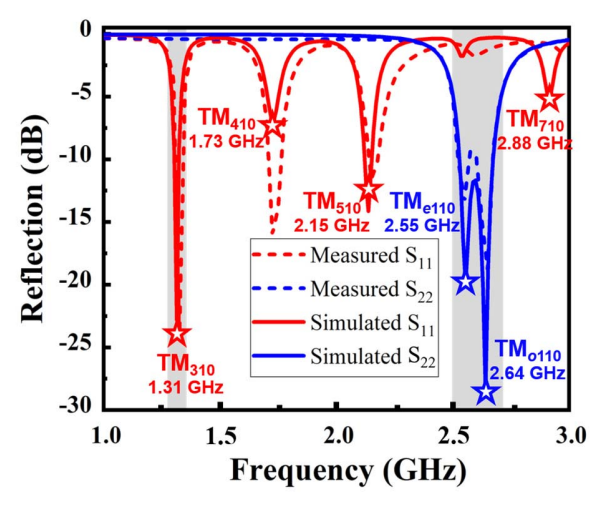


Fig. 5. Measured (dashed lines) and simulated (solid lines) reflection coefficient (S_{11} and S_{22}) for the antenna in Fig. 4. Analytical results obtained from Eqs. (1) and (2) are highlighted by stars.

TABLE I
DIMENSIONS OF THE PROPOSED ANTENNA IN FIG. 2 (UNIT: mm)

L = 85	$L_1 = 22$	W = 85	$W_1 = 22$	$h_1 = 1.5$
$h_2 = 1.5$	$h_3 = 0.1$	a = 16.5	b =15.675	$\theta_{\theta} = 30$
$R_2 = 38.2$	$R_3 = 22$	d = 4	$d_1 = 3.2$	$d_2 = 5$

simulation results. This measurement results confirm the dual-band behavior of the antenna, with a reflection dip at 1.33 GHz and a broadband resonance at its doubled frequency (2.5 GHz - 2.7 GHz). Although the harmonic sensor is designed to work in the S-band range (2 - 4 GHz), the concept and design can be readily transferred to other frequency bands. Fig. 6 reports the simulated and measured radiation patterns of the proposed microstrip antenna on the E- and H-planes at the fundamental frequency and the second-harmonic band. Note that for the TM₃₁₀ mode, the E-plane is yz-plane

TABLE II

COMPLEX PERMITTIVITIES OF DIFFERENT
ACETONE-WATER MIXTURES

Mixtures	0 %	20%	40%	60%	80%	100 %
	(acetone)					(water)
ε'_r	20.7	25	35	45	66	80
ε''_r	0.5	1	1.65	2.5	4.3	6

and the H-plane is xz-plane in 3D space, and those for the TM_{e110} (TM_{o110}) modes are yz- and xz-planes (xz- and yzplanes). The measured co-polarization radiation patterns with broadside radiation properties are in good agreement with the simulation results. At 1.33 GHz (TM₃₁₀ mode), this antenna exhibits a maximum measured gain of -1.5 dBi, with a halfpower beam width (HPBW) of 72° on the E-plane and a HPBW of 106° on H-plane. In the second-harmonic band, the TM_{e110} mode (2.52 GHz) and TM_{e110} mode (2.69 GHz) exhibit orthogonal linear polarizations, whereas circular polarizations are obtained between the two modes (2.6 GHz). At 2.52 GHz, the antenna exhibits a maximum gain of 4.5 dBi, with a HPBW of 84° (120°) on the E-plane (H-plane). At 2.69 GHz, the maximum antenna gain is 5.7 dBi, with a HPBW of 77° (115°) on the E-plane (H-plane). In these two cases, a high co-polarization discrimination is apparently seen, with a cross-polarization less than -15 dB (-10 dB) on the E-plane (H-plane). At 2.6 GHz, the antenna shows a maximum gain of 5.3 dBi and a HPBW of 86° (116°) on the E-plane (H-plane). In this case, the cross-polarization radiation pattern is similar to the co-polarization pattern, in light of intrinsic circular polarization properties of the elliptical patch. Due to relatively high dielectric and conduction losses in the FR4 substrate, the measured radiation efficiency is 27 % at 1.31 GHz and is greater than 80 % in the second-harmonic band. The realized gain of the proposed antennas can be further enhanced by selecting a high-quality substrate with minimum power dissipation.

Next, we will demonstrate the sensing function of the proposed reconfigurable dual-band antenna in terms of reflection spectrum. To this end, acetone and water mixtures with various concentrations were prepared with their complex permittivities listed in Table II [40]-[42]. Based on the perturbation theory [43], [44], the dielectric properties of the SUT filled into the fluidic cavity can be characterized by detecting the up- or down-shifting resonance frequency f_0 . In this study, to track the resonant frequency variation of the dual-band antenna, the Agilent N5222A PNA microwave network analyzer was used here to record the reflection spectrum of the antenna, i.e., S_{11} and S_{22} , and the measured reflection coefficients for acetone-water mixtures of different concentrations are shown in Fig. 7. It can be clearly seen that with the increase of the volume ratio of water to acetone (effectively, increasing the liquid's dielectric constant), the resonance frequency of the TM₃₁₀ mode downshifts from 1.325 GHz to 1.287 GHz, while the second-harmonic band (coupled TM_{e110} and TM_{o110} modes) remains unchanged (not shown here). The inset of Fig. 7 shows the simulated and measured resonance frequency of the TM₃₁₀ mode for different volume fractions of water in

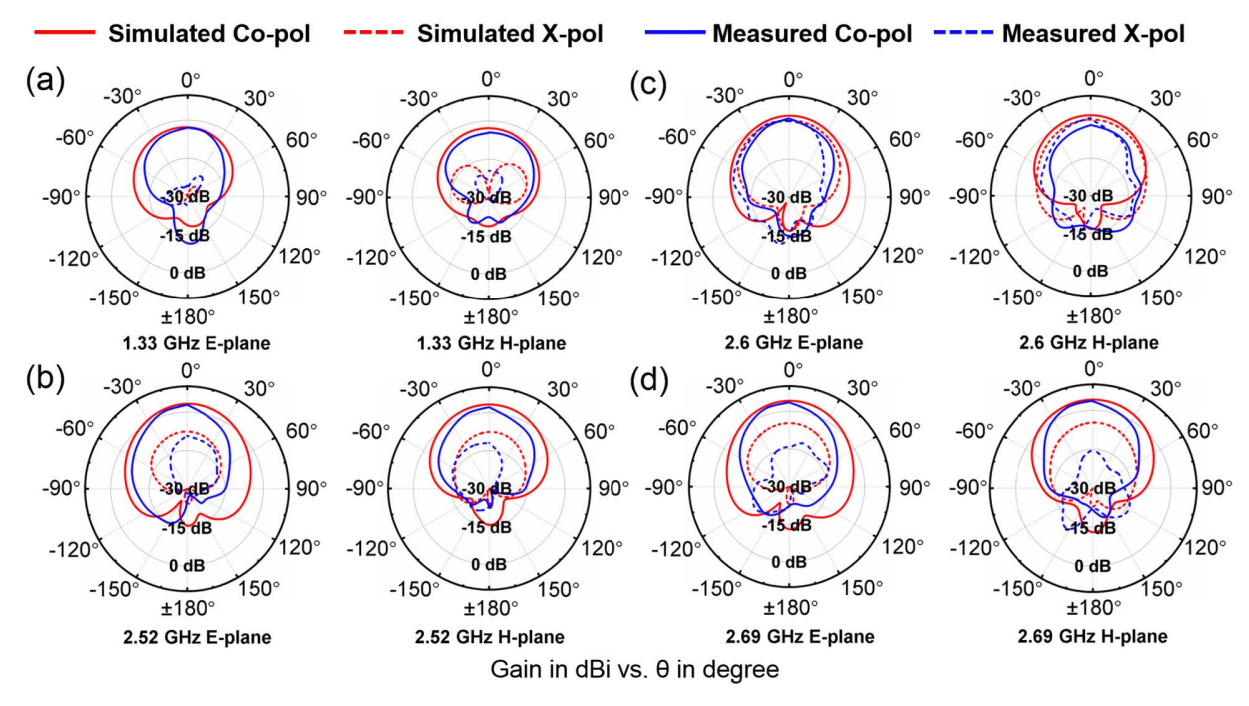


Fig. 6. Radiation patterns for the microstrip patch antenna in Fig. 4 on the E- and H-planes at: (a) 1.33 GHz, (b) 2.52 GHz, (c) 2.6 GHz, and (d) 2.69 GHz.

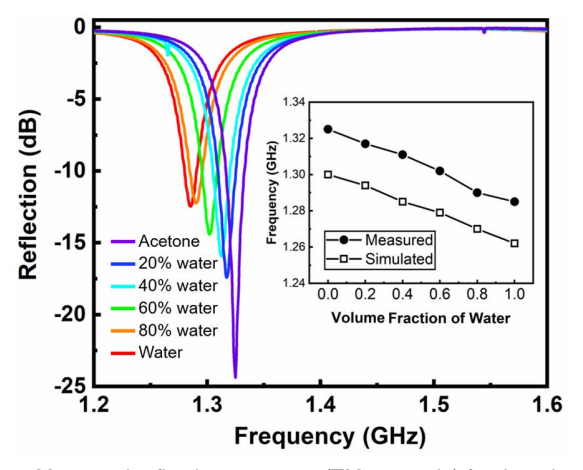


Fig. 7. Measured reflection spectrum (TM_{310} mode) for the microstrip patch antenna, loaded with the acetone-water mixture at different concentrations; the inset shows the measured and calculated resonance frequency f_0 against the volume fraction of water.

the mixture. It is evident that simulations and measurements are in good agreement, and both show excellent sensitivity and linearity in determination of volume fraction in binary liquid mixtures.

By connecting the aforementioned reconfigurable dual-band antenna to a passive frequency doubler [45], a fully passive wireless harmonic sensor can be built. Here, the bistatic radar measurement setup was used for the wireless sensor telemetry. The transceiver (T_x) continuously transmits the frequency-hopped RF signal with 20 channels to the harmonic sensor, which then resends the second harmonic to the sniffer device (R_x) . The envelope of these backscattered second harmonic tones recorded by the R_x forms the FHSS pattern, whose peak position depends on the effective dielectric constant of the loaded liquid mixtures, as shown in Fig. 8. This wireless far

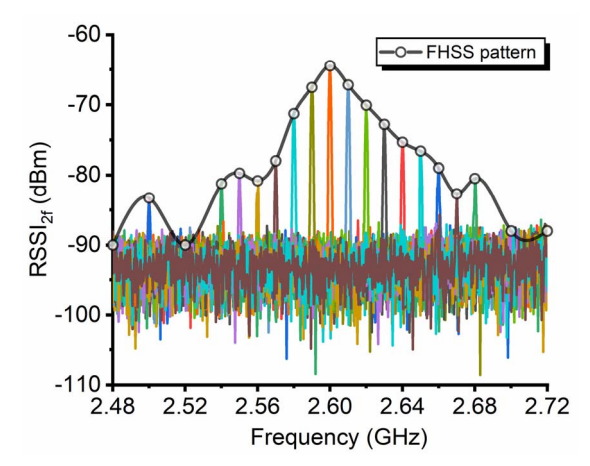


Fig. 8. Measured harmonic RSSI array for the water-acetone mixture (60 %), which was recorded by the spectrum analyzer connected to the sniffer R_X . The envelope of this RSSI array forms the FHSS pattern that contains sensing information for the fully-passive harmonic sensor.

field sensing mechanism can be comprehensively explained as below. According to the Friis transmission equation [46], the ratio of the power received by R_x to the power launched by T_x is given by:

$$\frac{P_r}{P_t} = \left(\frac{\lambda_0}{4\pi R_1}\right)^2 \cdot \left(\frac{\lambda_0/2}{4\pi R_2}\right)^2 \cdot \frac{G_1 G_2 G_T G_R}{L_{sys}} \cdot |\hat{\rho}_1 \cdot \hat{\rho}_t|^2 \cdot |\hat{\rho}_2 \cdot \hat{\rho}_r|^2, \quad (3)$$

where G_1 (G_2) is the realized gain of the dual-band antenna on the harmonic sensor at f_0 ($2f_0$), G_T (G_R) denotes the realized gain of the transceiver (sniffer) used to interrogate the passive sensor, R_1 (R_2) is the distance between T_x (R_x) and the harmonic sensor, L_{sys} is the system loss including the frequency-conversion loss and parasitics. Here, important

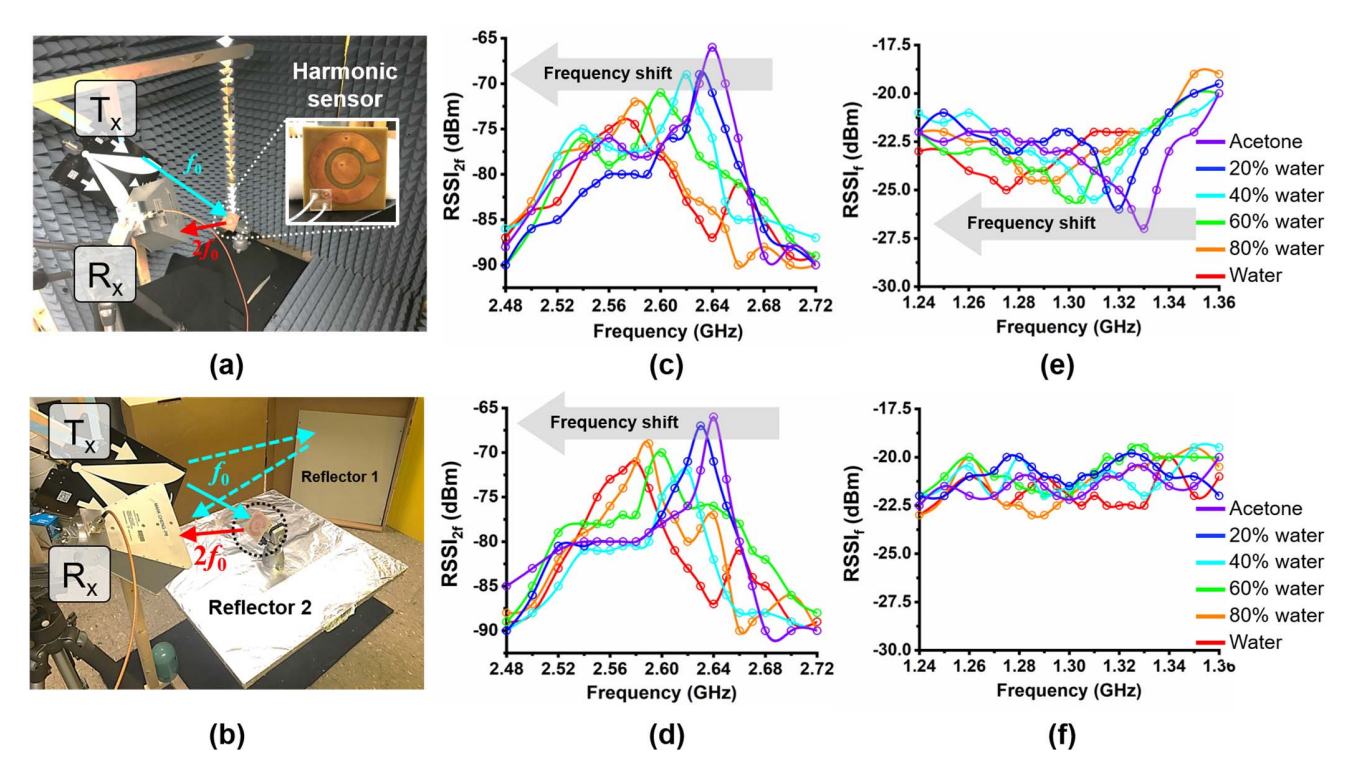


Fig. 9. Experimental setup for characterizing the wireless sensors: (a) interference-free environment (anechoic chamber) and (b) rich-scattering indoor environment. Measured FHSS pattern for the harmonic sensor in (c) interference-free and (d) rich-scattering environments. Determination of the volume fraction in acetone-water mixture is possible by tracking the peak frequency in the FHSS patterns. (e), (f) are similar to (c), (d), but for the linear backscatter sensor.

parameters are: $P_t = 25$ dBm, $R_1 = R_2 = 1.0$ m, $G_T = 5.5$ dBi at 1.1 GHz and $G_R = 12$ dBi at 2.6 GHz. In Eq. (3), $|\hat{\rho}_1 \cdot \hat{\rho}_t|^2$ is the polarization coupling factor between the T_x antenna and the harmonic sensor, which is approximately equal to unity if the two antennas are well aligned. On the other hand, $|\hat{\rho}_2 \cdot \hat{\rho}_r|^2$ accounts for the polarization match between the R_x antenna and the harmonic sensor. Since the TM_{e110} mode and TM_{o110} modes excited in the second-harmonic band have orthogonal polarizations [see Figs. 3 and 6], the R_x antenna is titled by 45° to capture radiation produced by both modes; here, $|\hat{\rho}_2 \cdot \hat{\rho}_r|^2$ is ~ 50 % in the entire second-harmonic band. In summary, according to Eq. (3), the received power P_r and RSSI are proportional to the realized gain G_1 and G_2 , in which G_2 remains almost constant with a ± 0.5 dB fluctuation, while G_1 is quite sensitive to the concentration of the acetone-water mixture. When the acetone concentration decreases, which is corresponding to the increase of the dielectric constant of the mixture, the frequency of peak G_1 is shifted from 1.325 GHz to 1.287 GHz [see Fig. 7], leading to the FHSS pattern downshift as can be seen in Fig. 9(c) (measured in an anechoic chamber) and Fig. 9(d) (measured in a rich-scattering indoor environment). It is evidently seen that the peak RSSI of FHSS pattern is sensitively shifted from 2.642 GHz to 2.58 GHz and that such a trend is independent of the density of the electromagnetic environment. In this work, for comparison, we also employed the conventional passive backscatter sensor to wirelessly monitor the same liquid mixtures. In this case, the dual-band microstrip antenna is disconnected from the

frequency doubler and its port 1 (labeled in Fig. 2(b)) is terminated by a 50 Ω match load. We notice that in passive scattering events, the extinction cross section is the sum of absorption and scattering cross sections. A dip in RSSI and RCS spectrum is sometimes observed at the resonance. In this case, the incident power is absorbed without causing too much scattering; namely, the absorption cross section is greater than the scattering cross section [47]. Figs. 9(e) and 9(f) report the measured FHSS pattern for the conventional backscatter sensor placed in the anechoic chamber and the noisy environment, respectively. Although the backscatter sensor can function well in a noise-free anechoic chamber, it fails to comprehensively detect the liquid properties in rich-scattering environments involving echoes, clutters, multipath scattering, and the possible crosstalk between T_x and R_x . Apparently, compared to conventional backscatter sensors, our proposed frequency-hopping harmonic sensor can robustly and sensitively detect dielectric properties of liquid mixtures, regardless of background interferences. Fig. 10 summarizes the measured peak values of FHSS pattern as a function of the water volume fraction in different scattering-rich environments. It is evident that increasing the number of large PEC scatters surrounding the harmonic sensor would not affect the sensing performance, which further demonstrates the robustness and effectiveness of our frequency-hopping harmonic sensor. Moreover, we can define our sensitivity as the slope of the curve, i.e., -0.62 MHz/1%, which means when the volume fraction of water is increased by 1%, the peak of the FHSS pattern will be downshifted by 0.62 MHz. Such sensitivity

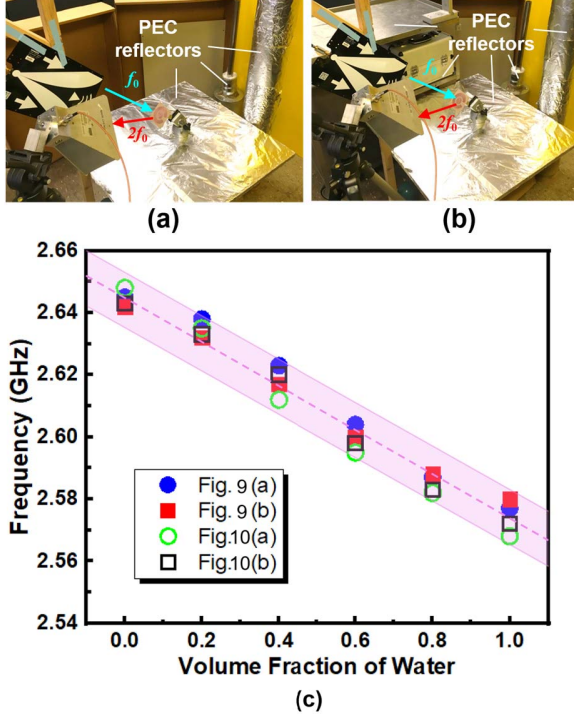


Fig. 10. Experimental setup in rich-scattering indoor environment with (a) two more metal reflectors and (b) six metal reflectors. (c) Peak frequency against the volume fraction of water in the acetone-water mixture; here, data was obtained using the harmonic sensor placed in different environments including Figs. 9(a) and 9(b).

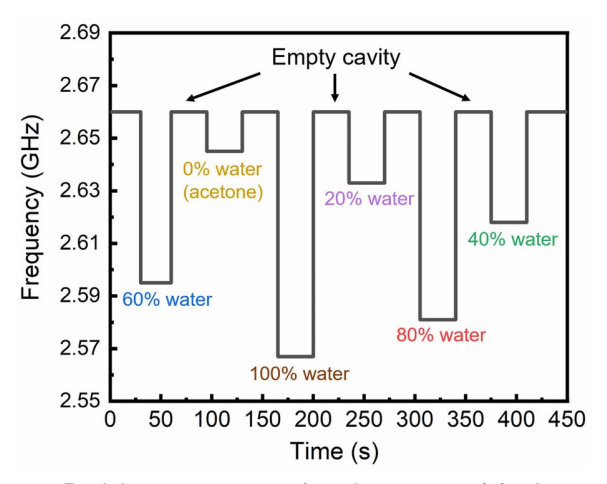


Fig. 11. Real time measurement (transient response) for the passive harmonic sensor working in a noisy environment (Fig. 10(b)); here, different acetone-water mixtures were injected in and removed from the fluidic cavity every minute, with a 30 s interval for the empty state reference.

and resolvability allow us to differentiate two liquids with a difference of 5% water.

Finally, we have validated the repeatability and real time capability (transient response) of this harmonic sensor working in a noisy environment. Here, different acetone-water mixtures were injected in and removed from the fluidic cavity every minute, with a 30 s interval for the empty state reference. The measurement results reported in Fig. 11 clarify that the sensor can always restore to its original state (with a peak RSSI at 2.66 GHz) after several operating cycles. Such a robust and repeatable wireless sensing capability may enable many

biological and healthcare monitoring applications, such as the wireless passive lab-on-chip platforms. We should also note that the proposed compact harmonic sensor may be integrated with more complex fluidic channels and diagnostic assays to maximize its potential for high-performance wireless sensing and telemetering.

IV. CONCLUSION

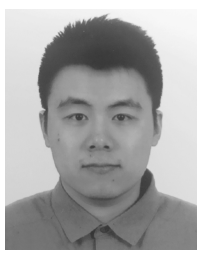
We have proposed a low-profile, reconfigurable dual-band microstrip antenna for realizing far field wireless frequency-hopping harmonic sensors. The proposed microstrip antenna, loaded appropriately with a fluidic channel, can exhibit a tunable narrow resonance at the fundamental frequency and an invariant wideband resonance at the second-harmonic frequency. We have demonstrated that such an antenna is particularly useful for the frequency-hopping telemetry scheme, which allows for robust wireless liquid sensing in noisy environments (e.g., dense urban and indoor areas). The implementation of compact zero-power harmonic sensors with the capability of noise suppression may pave the way towards future integrated IoT sensors and battery-less smart RFID tags.

REFERENCES

- [1] X. Jia, Q. Feng, T. Fan, and Q. Lei, "RFID technology and its applications in Internet of Things (IoT)," in *Proc. 2nd Int. Conf. Consum. Electron.*, Commun. Netw. (CECNet), Apr. 2012, pp. 1282–1285.
- [2] E. Welbourne et al., "Building the Internet of Things using RFID: The RFID ecosystem experience," *IEEE Internet Comput.*, vol. 13, no. 3, pp. 48–55, May 2009.
- [3] G. Bedi, G. K. Venayagamoorthy, R. Singh, R. R. Brooks, and K.-C. Wang, "Review of Internet of Things (IoT) in electric power and energy systems," *IEEE Internet Things J.*, vol. 5, no. 2, pp. 847–870, Apr. 2018.
- [4] S. Amendola, R. Lodato, S. Manzari, C. Occhiuzzi, and G. Marrocco, "RFID technology for IoT-based personal healthcare in smart spaces," *IEEE Internet Things J.*, vol. 1, no. 2, pp. 144–152, Apr. 2014.
- [5] S. Preradovic, I. Balbin, N. C. Karmakar, and G. F. Swiegers, "Multiresonator-based chipless RFID system for low-cost item tracking," *IEEE Trans. Microw. Theory Techn.*, vol. 57, no. 5, pp. 1411–1419, May 2009.
- [6] K. G. Ong, K. F. Zeng, and C. A. Grimes, "A wireless, passive carbon nanotube-based gas sensor," *IEEE Sensors J.*, vol. 2, no. 2, pp. 82–88, Apr. 2002
- [7] R. Bhattacharyya, C. Floerkemeier, and S. Sarma, "Low-cost, ubiquitous RFID-tag-antenna-based sensing," *Proc. IEEE*, vol. 98, no. 9, pp. 1593–1600, Sep. 2010.
- [8] F. Alimenti and L. Roselli, "Theory of zero-power RFID sensors based on harmonic generation and orthogonally polarized antennas," *Prog. Electromagn. Res.*, vol. 134, 337-357, 2013.
- [9] K. Rasilainen, J. Ilvonen, A. Lehtovuori, J.-M. Hannula, and V. Viikari, "Harmonic transponders: Performance and challenges," *Prog. Electro-magn. Res. M*, vol. 41, pp. 139–147, 2015.
- [10] K. Rasilainen, J. Ilvonen, and V. Viikari, "Antenna matching at harmonic frequencies to complex load impedance," *IEEE Antennas Wireless Propag. Lett.*, vol. 14, pp. 535–538, 2015.
- [11] K. Rasilainen, J. Ilvonen, A. Lehtovuori, J.-M. Hannula, and V. Viikari, "On design and evaluation of harmonic transponders," *IEEE Trans. Antennas Propag.*, vol. 63, no. 1, pp. 15–23, Jan. 2015.
- [12] X. Gu, N. N. Srinaga, L. Guo, S. Hemour, and K. Wu, "Diplexer-based fully passive harmonic transponder for sub-6-GHz 5G-compatible IoT applications," *IEEE Trans. Microw. Theory Techn.*, vol. 67, no. 5, pp. 1675–1687, May 2019.
- [13] Y. Feng, Y. Li, L. Li, B. Ma, H. Hao, and L. Li, "Tissue-dependent co-matching method for dual-mode antenna in implantable neurostimulators," *IEEE Trans. Antennas Propag.*, vol. 67, no. 8, pp. 5253–5264, Aug. 2019.
- [14] Y. Li, Z. Zhang, W. Chen, Z. Feng, and M. F. Iskander, "A switchable matching circuit for compact wideband antenna designs," *IEEE Trans. Antennas Propag.*, vol. 58, no. 11, pp. 3450–3457, Nov. 2010.

- [15] Y. Li, Z. Zhang, W. Chen, Z. Feng, and M. F. Iskander, "A compact DVB-H antenna with varactor-tuned matching circuit," *Microw. Opt. Technol. Lett.*, vol. 52, no. 8, pp. 1786–1789, Aug. 2010.
- [16] Y. Feng, Y. Li, L. Li, B. Ma, H. Hao, and L. Li, "Design and system verification of reconfigurable matching circuits for implantable antennas in tissues with broad permittivity range," *IEEE Trans. Antennas Propag.*, vol. 68, no. 6, pp. 4955–4960, Jun. 2020.
- [17] B. G. Colpitts and G. Boiteau, "Harmonic radar transceiver design: Miniature tags for insect tracking," *IEEE Trans. Antennas Propag.*, vol. 52, no. 11, pp. 2825–2832, Nov. 2004.
- [18] D. Mascanzoni and H. Wallin, "The harmonic radar: A new method of tracing insects in the field," *Ecol. Entomol.*, vol. 11, no. 4, pp. 387–390, 1986
- [19] J. R. Riley et al., "Tracking bees with harmonic radar," Nature, vol. 379, no. 6560, pp. 29–30, Jan. 1996.
- [20] D. Psychoudakis, W. Moulder, C.-C. Chen, H. Zhu, and J. L. Volakis, "A portable low-power harmonic radar system and conformal tag for insect tracking," *IEEE Antennas Wireless Propag. Lett.*, vol. 7, pp. 444–447, 2008
- [21] J. L. Osborne *et al.*, "A landscape-scale study of bumble bee foraging range and constancy, using harmonic radar," *J. Appl. Ecol.*, vol. 36, no. 4, pp. 519–533, Sep. 1999.
- [22] C. Van Tilburg et al., "Wilderness medical society practice guidelines for prevention and management of avalanche and nonavalanche snow burial accidents," Wilderness Environ. Med., vol. 28, no. 1, pp. 23–42, Mar. 2017.
- [23] M. Hajizadegan et al., "Graphene sensing modulator: Toward low-noise, self-powered wireless microsensors," *IEEE Sensors J.*, vol. 17, no. 22, pp. 7239–7247, Nov. 2017.
- [24] H. Huang, P. Y. Chen, C. H. Hung, R. Gharpurey, and D. Akinwande, "A zero power harmonic transponder sensor for ubiquitous wireless μL liquid-volume monitoring," Sci. Rep., vol. 6, p. 18795, Jan. 2016.
- [25] H. Huang, M. Sakhdari, M. Hajizadegan, A. Shahini, D. Akinwande, and P.-Y. Chen, "Toward transparent and self-activated graphene harmonic transponder sensors," *Appl. Phys. Lett.*, vol. 108, no. 17, Apr. 2016, Art. no. 173503.
- [26] A. Lazaro, R. Villarino, and D. Girbau, "A passive harmonic tag for humidity sensing," *Int. J. Antennas Propag.*, vol. 2014, Jul. 2014, Art. no. 670345.
- [27] H. Huang et al., "Chemical-sensitive graphene modulator with a memory effect for internet-of-things applications," *Microsyst. Nanoeng.*, vol. 2, p. 16018, May 2016.
- [28] D. Ahbe, S. Beer, T. Zwick, Y. Wang, and M. M. Tentzeris, "Dual-band antennas for frequency-doubler-based wireless strain sensing," *IEEE Antennas Wireless Propag. Lett.*, vol. 11, pp. 216–219, 2012.
- [29] C. Cho, X. Yi, D. Li, Y. Wang, and M. M. Tentzeris, "Passive wireless frequency doubling antenna sensor for strain and crack sensing," *IEEE Sensors J.*, vol. 16, no. 14, pp. 5725–5733, Jul. 2016.
- [30] L. Zhu, N. Alkhaldi, H. M. Kadry, S. Liao, and P.-Y. Chen, "A compact hybrid-fed microstrip antenna for harmonics-based radar and sensor systems," *IEEE Antennas Wireless Propag. Lett.*, vol. 17, no. 12, pp. 2444–2448, Dec. 2018.
- [31] L. Zhu and P.-Y. Chen, "A compact, zero-power and low-noise harmonic-transponder for liquid and moisture sensing," in *Proc. IEEE Int. Symp. Antennas Propag. USNC-URSI Radio Sci. Meeting*, Jul. 2019, pp. 1109–1110.
- [32] K. Carver and J. Mink, "Microstrip antenna technology," *IEEE Trans. Antennas Propag.*, vol. 29, no. 1, pp. 2–24, Jan. 1981.
- [33] W. Richards, Y. Lo, and D. Harrison, "An improved theory for microstrip antennas and applications," *IEEE Trans. Antennas Propag.*, vol. 29, no. 1, pp. 38–46, Jan. 1981.
- [34] D. M. Pozar, Microwave Engineering, 4th ed. Hoboken, NJ, USA: Wiley, 2012.
- [35] J. C. Gutiérrez-Vega, R. M. Rodríguez-Dagnino, M. A. Meneses-Nava, and S. Chávez-Cerda, "Mathieu functions, a visual approach," *Amer. J. Phys.*, vol. 71, no. 3, pp. 233–242, Mar. 2003.
- [36] D. A. Goldberg, L. J. Laslett, and R. A. Rimmer, "Modes of elliptical waveguides: A correction," *IEEE Trans. Microw. Theory Techn.*, vol. 38, no. 11, pp. 1603–1608, Nov. 1990.
- [37] P. Y. Chen and A. Alu, "Dual-mode miniaturized elliptical patch antenna with μ-negative metamaterials," *IEEE Antennas Wireless Propag. Lett.*, vol. 9, pp. 351–354, 2010.
- [38] P. Y. Chen and A. Alù, "Sub-wavelength elliptical patch antenna loaded with μ-negative metamaterials," *IEEE Trans. Antennas Propag.*, vol. 58, no. 9, pp. 2909–2919, Sep. 2010.
- [39] ANSYS 2020 R1 Academic Research Electromagnetics Suite, ANSYS, Inc., Canonsburg, PA, USA, 2020.

- [40] C. Malmberg and A. Maryott, "Dielectric constant of water from 0" to 100°C," J. Res. Nat. Bur. Standards, vol. 56, pp. 1–8, 1956.
- [41] G. Akerlöf, "Dielectric constants of some organic solvent-water mixtures at various temperatures," *J. Amer. Chem. Soc.*, vol. 54, no. 11, pp. 4125–4139, 1932.
- [42] C. Gao, T. Wei, F. Duewer, Y. Lu, and X.-D. Xiang, "High spatial resolution quantitative microwave impedance microscopy by a scanning tip microwave near-field microscope," *Appl. Phys. Lett.*, vol. 71, no. 13, pp. 1872–1874, Sep. 1997.
- [43] K. Saeed, R. D. Pollard, and I. C. Hunter, "Substrate integrated waveguide cavity resonators for complex permittivity characterization of materials," *IEEE Trans. Microw. Theory Techn.*, vol. 56, no. 10, pp. 2340–2347, Oct. 2008.
- [44] H. Huang et al., "RFID tag Helix antenna sensors for wireless drug dosage monitoring," IEEE J. Transl. Eng. Health Med., vol. 2, pp. 1–8, Mar. 2014, Art. no. 1700108.
- [45] FK-3000+ From Mini-Circuit. Accessed: Mar. 14, 2019. [Online]. Available: http://www.minicircuits.com/WebStore/dashboard_html?model=FK-3000%2B
- [46] J. A. Shaw, "Radiometry and the Friis transmission equation," Amer. J. Phys., vol. 81, no. 1, pp. 33–37, Jan. 2013.
- [47] A. M. J. Marindra and G. Y. Tian, "Chipless RFID sensor tag for metal crack detection and characterization," *IEEE Trans. Microw. Theory Techn.*, vol. 66, no. 5, pp. 2452–2462, May 2018.



Liang Zhu (Graduate Student Member, IEEE) received the M.Sc. degree in optics from Sun Yat-sen University, Guangzhou, China, in 2015. He is currently pursuing the Ph.D. degree in electrical engineering with the University of Illinois, Chicago. His research interests include RF/microwave antennas and circuits, energy harvesting platforms, and wireless sensors.



Mohamed Farhat received the master's degree in theoretical physics and the Ph.D. degree in optics and electromagnetism from Aix-Marseille University, France. He has authored over than 150 publications: 70 journal articles, six book chapters, five international patents, four proceedings, and over 70 conference papers (with more than 3300 citations and H-index 30, from Google Scholar, as of May 2020). He has also co-edited the book *Transformation Wave Physics: Electromagnetics, Elastodynamics and Thermodynam-*

ics (Pan Stanford Publishing). His research interests include plasmonics and metamaterials with applications spanning optics and acoustics waves. He is an Active Reviewer for many international journals in physics, including *Physical Review Letters* and *Nature Physics*. He has organized several special sessions at the conferences Meta'13, Meta'14, Meta'15, Meta'16, Meta'17, and Meta'18.



Yi-Chao Chen (Member, IEEE) received the Ph.D. degree in computer science from The University of Texas at Austin in 2015. He was a tenure-track Associate Professor with the Department of Computer Science and Engineering, Shanghai Jiao Tong University (SJTU), in 2018. Prior to joining SJTU, he worked as a Co-Founder with Hauoli LLC. His research interests include networked systems and span the areas of mobile computing, wireless networking, and cyber-security.



Khaled N. Salama (Senior Member, IEEE) received the B.S. degree from the Department of Electronics and Communications, Cairo University, Cairo, Egypt, in 1997, and the M.S. and Ph.D. degrees from the Department of Electrical Engineering, Stanford University, Stanford, CA, USA, in 2000 and 2005, respectively. He was an Assistant Professor with the Rensselaer Polytechnic Institute, NY, USA, from 2005 to 2009. He joined the King Abdullah University of Science and Technology (KAUST) in January 2009,

where he is currently a Professor, and was the Founding Program Chair until August 2011. He is the Director of the Sensors Initiative, a consortium of nine universities. His work on CMOS sensors for molecular detection has been funded by the National Institutes of Health (NIH) and the Defense Advanced Research Projects Agency (DARPA), awarded the Stanford–Berkeley Innovators Challenge Award in biological sciences and was acquired by Illumina Inc. He is the author of 250 articles and 14 U.S. patents on low-power mixed signal circuits for intelligent fully integrated sensors and neuromorphic circuits using memristor devices.



Pai-Yen Chen (Senior Member, IEEE) received the Ph.D. degree from The University of Texas at Austin in 2013. He was a Research Scientist with the Intellectual Ventures' Metamaterial Commercialization Center from 2013 to 2014 and a Research Staff with the National Nano Device Laboratory, Taiwan, from 2006 to 2009. He is an Associate Professor with the Department of Electrical and Computer Engineering, University of Illinois, Chicago. He has been involved in multidisciplinary research on applied electro-

magnetics, RF/microwave antennas and circuits, wireless micro/nanosensors and integrated systems, as well as nanoelectromagnetism in plasmonics and nanophotonics. He has received guite a few prestigious awards, including the National Science Foundation (NSF) Career Award, the IEEE Sensors Council Young Professional Award, the IEEE Raj Mittra Travel Grant (RMTG) Award, the SPIE Rising Researcher Award, the ACES Early Career Award, the PIERS Young Professional Award, the Young Scientist Awards from URSI General Assembly and URSI Commission B: Electromagnetics, the Air Force Research Laboratory Faculty Fellowship, the National Argonne Laboratory Director's Fellowship, the College of Engineering Faculty Research Excellence Award, the Donald Harrington Fellowship, the Taiwan Ministry of Education Study Abroad Award, the United Microelectronics Corporation Scholarship, and quite a few student paper awards and travel grants from major IEEE conferences, including the USNC-URSI Ernest K. Smith Student Paper Award. He currently serves as an Associate Editor of the IEEE SENSORS JOURNAL, the IEEE JOURNAL OF RADIO FREQUENCY IDENTIFICATION (IEEE JRFID), the IEEE JOURNAL OF ELECTROMAGNETICS, RF AND MICROWAVES IN MEDICINE AND BIOLOGY (IEEE-JERM), and a guest editor of several international journals. He was a former Associate Editor of Applied Electromagnetics.